CARBON 84 (2015) 263–271

Available at www.sciencedirect.com

ScienceDirect

journal homepage: www.elsevier.com/locate/carbon

Mechanics of nanoscale wrinkling of graphene on a non-developable surface

Yanguang Zhou [a,c,d], Yuli Chen [a,*], Bin Liu [b], Shengtao Wang [a], Zhenyu Yang [a], Ming Hu [c,d]

[a] Institute of Solid Mechanics, Beihang University (BUAA), Beijing 100191, China
[b] AML, Department of Engineering Mechanics, Tsinghua University, Beijing 100084, China
[c] Institute of Mineral Engineering, Division of Materials Science and Engineering, Faculty of Georesources and Materials Engineering, Rheinisch-Westfaelische Technische Hochschule (RWTH Aachen University), 52064 Aachen, Germany
[d] Aachen Institute for Advanced Study in Computational Engineering Science (AICES), RWTH Aachen University, 52062 Aachen, Germany

ARTICLE INFO

Article history:
Received 19 August 2014
Accepted 20 November 2014
Available online 3 December 2014

ABSTRACT

As a two-dimensional crystal, the graphene sheet is often used with substrate materials because the freestanding graphene tends to corrugate and can hardly display its extraordinary properties in devices. However, the substrate is rarely perfectly-flat, but has microscopic roughness. Whether or not the graphene sheet can conform fully to a substrate with nano- and micro-roughness is essential for the performance of the graphene-based devices. In this paper, a theoretical model is developed to predict the morphology of a monolayer graphene sheet attaching to the substrate with microscopic non-developable roughness by an energy-based analysis. The final graphene morphology is revealed to result from the competition between two energy terms: the adhesion energy between graphene and substrate, and the strain energy stored in the graphene due to the deformations. Thus, by accounting for these two parts of energy, the critical condition to predict the morphology conversion from full conformation to wrinkling is established, which agrees well with the results of molecular dynamics simulations. This study has significant meanings for design and fabrication of high quality nanostructured coatings on substrates with complex surfaces, and can offer a guide for designing new functional graphene electronical devices such as nano-sensors and nano-switches as well.

1. Introduction

The graphene, a two-dimensional crystal with hexagonally arranged and covalently bonded carbon atoms, has attracted widespread concern in recent years due to its great potential applications in nano-electronics [1], nano-electromechanical systems [2,3] and composite materials [4,5]. The freestanding graphene is non-flat and tends to be corrugated due to the instability of its molecular structure, such as intrinsically thermal fluctuation [6], so graphene is often used with substrate materials as a coating layer [7,8]. However, wrinkles often appear in the graphene due to the structural mismatch between the graphene and the substrate [9–14], and the wrinkling morphology of graphene impacts significantly on its electronic [15,16] and mechanical properties [11,17–19].

Therefore, it is of great importance to know whether or not the graphene sheet can conform to the substrate fully and smoothly and to understand the mechanism of the formation of wrinkles in graphene sheets. The morphology of graphene can change the electronic properties of graphene via changing the scattering of charge carriers [20,21]. On one hand,

* *Corresponding author:* Fax: +86(0)10 8233 9228.
E-mail address: yulichen@buaa.edu.cn (Y. Chen).
http://dx.doi.org/10.1016/j.carbon.2014.11.055
0008-6223/

since it needs high carrier mobility for some nano-electronic applications, atomically flat substrates [22–24] are introduced to form morphology of graphene without extrinsic wrinkles, which can reduce the charge inhomogeneity [25]. On the other hand, some simulations [26,27] and experiments [28] have predicted that wrinkles can enhance the chemical activity of graphene, and form nanosized gas inlet for chemical reactions [29–31], so the wrinkled graphene can be a good candidate for nano-sensors and nanoswitches.

The substrates can rarely perfectly-flat, but with nano- and/or micro-roughness. So the graphene morphology on the substrates with these asperities is essential for the performance of the graphene-based devices. Previous studies are mainly focused on the conformation of graphene sheet on a substrate with developable surface, such as corrugated substrate [32–35]. However, the micro- and nano-roughness of substrates can hardly be modeled by developable surfaces, so the behavior of graphene sheets on non-developed surfaces still needs investigation. Furthermore, increasing applications of graphene-like sheet attaching to non-developable surfaces are reported [36–39]. For example, the remarkable study on electronic eye camera requires full conformation of silicon sheet to a hemispherical surface [24], and experiments show that coating graphene onto the tip of atomic force microscope (AFM) can improve the device lifetime and protect the sample materials [13,14]. Therefore, it is desirable to build a theoretical model to predict the final morphology of the graphene on the substrate with non-developable surfaces.

The purpose of this paper is to establish a mechanics theory for the conformation of graphene sheets to the macro-flat substrate with non-developable nano- and micro-roughness. A simple criterion on the full-conformation/wrinkling of graphene is obtained, which agrees well with the subsequent MD simulations. Both the theoretical predictions and MD results show that the final morphologies of graphene are only related to the absorbed cone angle, which is determined by the curvature and area of the substrate asperities.

2. Morphology of graphene sheet conforming to substrate with asperities

If the substrate is perfectly flat, graphene sheets can easily conforms to the substrate. However, most substrates are not perfect, but have nano- and/or micro-asperities. It has been proved that the generation of wrinkles is determined by the morphology of the substrate [40]. Here, the asperities are simplified and simulated as dome-shaped bumps distributed on the surface of substrates. MD simulations on conforming behavior of monolayer graphene sheets to rough SiO_2 substrates show two typical morphologies (see Section 4 for more details about MD simulations), as presented in Fig. 1. In Fig. 1(a), the graphene sheet conforms to the substrate well, but in Fig. 1(b), the graphene sheet conforms partially and wrinkles at the edges of the dome-shaped bumps of the substrate.

It should be noted that the domes on the two substrates in Fig. 1(a) and (b) have the same distance (D = 40 nm) and height (H = 5 nm). Then what dominates the morphology of graphene, and what is the mechanism of the conforming behavior? To answer these questions, a theoretical model will be developed in the following section.

3. Theoretical analysis on graphene conforming to a dome-shaped bump

Some previous studies have been carried out for the adhesion of continuum thin elastic plate and elastic sheet to a spherical surface [41,42]. Especially, Majidi and Fearing established an analytical expression about the adhesion of thin elastic plate to a rigid sphere based on stationary principles and the von Karman plate theory [41]. However, their model is not suitable for the graphene-substrate system due to their assumptions of constant adhesion energy density and small ratio of graphene radius to substrate radius. In this section, a theoretical model is established based on the energy method to predict the final morphology of the graphene on the substrate with non-developable nano- and micro-asperities.

3.1. *Theoretical model*

For a substrate scattered with bumps with sufficient distance between each pair of them, it can be observed from Fig. 1 that the dome region is the most important part that causes different morphologies of graphene. So a model consisting of a round graphene sheet and a dome-shaped bump is established, as shown in Fig. 2. According to the morphology observed in Fig. 1(a), the full conforming process can be imaged as follows. The round graphene sheet first deforms into a spherical cap and then covers the dome-shaped bump by the interactions between the graphene and the substrate, as demonstrated in Fig. 2. A spherical coordinate system (r, θ, φ) is set up at the center of the spherical substrate.

3.2. *Energy analysis*

To establish the critical condition to judge whether a monolayer graphene sheet can fully conform to the un-developable rounded bumps, an energy-based analysis is carried out. The total system energy E_T consists of three parts: (1) the graphene membrane energy E_m, (2) the bending energy E_b due to the change of graphene curvature, and (3) the graphene-substrate adhesion energy E_{ad}. The substrate is treated as a rigid and its strain energy can be ignored because the substrate is much thicker than the graphene and thus the deformation is constrained by the lower-layer material.

3.2.1. *Membrane energy of fully conformed graphene*

For the graphene fully conformed to a spherical substrate, the membrane energy of the graphene sheet is not negligible because the sphere surface is non-developable and thus leads to significant in-plane deformations of graphene. Here, the membrane energy of the graphene sheet, E_m, is determined by the tangential strain $\varepsilon_{\theta\theta}$ and the hoop strain $\varepsilon_{\varphi\varphi}$, which are defined in the spherical coordinate system (r, θ, φ), as shown in Fig. 2(d). The shear stress is ignored due to the symmetry of the system.

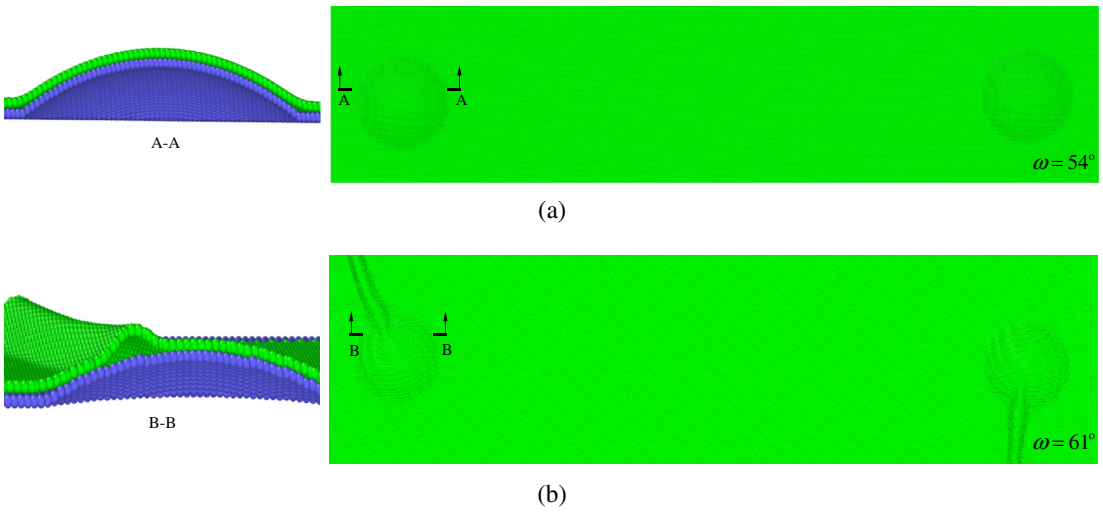

Fig. 1 – The final morphologies of the graphene on a substrate with dome-shaped bumps with the same distance and height but different absorbed cone angles: (a) full conformation, (b) wrinkling. (A color version of this figure can be viewed online.)

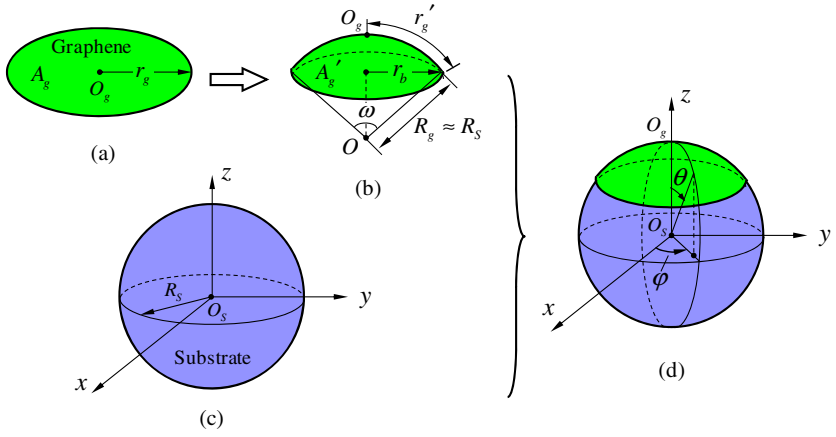

Fig. 2 – Model of graphene-substrate system: (a) the initial morphology of graphene: r_g and A_g are the radius and area of graphene, respectively, (b) the fully conformed morphology of graphene: r_b is the base radius of the spherical cap, r'_g and A'_g is the arc length and area of the deformed graphene, respectively, and ω is the absorbed cone angle, (c) the spherical substrate: R_S is the radius of substrate, (d) the schematic of a graphene sheet conforming fully to the spherical substrate. (A color version of this figure can be viewed online.)

According to the MD simulation in Appendix A, the area of a graphene sheet fully conformed to the substrate surface is at most 0.64% smaller than its initial area. So it is reasonable to assume the area of graphene is unchanged during it conforming to the substrate, i.e.

$$A'_g = A_g \tag{1}$$

in which A_g and A'_g are the areas of graphene sheet at the initial and fully conformed states, respectively, expressed as

$$A_g = \pi r_g^2 \tag{2}$$

$$A'_g = 2\pi R_S^2 - 2\pi R_S z, \quad z \in \left(R_S - \frac{r_g{}^2}{2R_S}, R_S\right) \tag{3}$$

where r_g and R_S are the radius of graphene and substrate, respectively, and z is the coordinate of z-axis, as shown in Fig. 2.

Substituting Eqs. (2) and (3) into Eq. (1), the initial radius of graphene sheet r_g can be expressed as a function of z as

$$r_g = \sqrt{2R_S^2 - 2R_S z} \tag{4}$$

As illustrated in Fig. 2, after full conformation, the flat graphene becomes a spherical cap with a base radius r_b, and the initial radius of graphene sheet r_g deformed to the arc length r'_g. The radius of the base of the cap r_b and the arc length r'_g can be obtained as

$$r_b = \sqrt{R_S^2 - z^2} \tag{5}$$

$$r'_g = R_S \arccos\left(\frac{z}{R_S}\right) \tag{6}$$

Thus, the tangential strain $\varepsilon_{\theta\theta}$ and the hoop strain $\varepsilon_{\varphi\varphi}$ can be described as

$$\varepsilon_{\theta\theta} = \frac{dr'_g - dr_g}{dr_g} = \frac{\sqrt{2R_S}}{\sqrt{R_S + z}} - 1 \tag{7}$$

$$\varepsilon_{\varphi\varphi} = \frac{2\pi r_b - 2\pi r_g}{2\pi r_g} = \frac{\sqrt{R_S + z}}{\sqrt{2R_S}} - 1 \tag{8}$$

The membrane energy of the graphene due to the in-plane stretching is

$$E_m = \frac{Et_g}{2(1-\nu^2)} \int_{A'_g} \left(\varepsilon_{\theta\theta}^2 + 2\nu\varepsilon_{\theta\theta}\varepsilon_{\varphi\varphi} + \varepsilon_{\varphi\varphi}^2\right) dA'_g \tag{9}$$

where E and ν are the Young's modulus and the Poisson's ratio of the graphene, respectively, and t_g is the thickness of the graphene sheet, which is generally considered to be 0.34 nm [3].

Substituting Eqs. (3), (7) and (8) into Eq. (9), the membrane energy of the graphene conformed to the spherical substrate is obtained as

$$\begin{aligned} E_m = \frac{2\pi R_S^2 E t_g}{(1-\nu^2)} \Bigg\{ & 4(1+\nu)\left[\sqrt{1-\left(\frac{r_g}{2R_S}\right)^2} + \frac{1}{3}\left(\sqrt{1-\left(\frac{r_g}{2R_S}\right)^2}\right)^3\right] \\ & - \ln\left[1-\left(\frac{r_g}{2R_S}\right)^2\right] \\ & - \frac{1}{2}\left[1-\left(\frac{r_g}{2R_S}\right)^2\right]^2 - 2(1+2\nu)\left[1-\left(\frac{r_g}{2R_S}\right)^2\right] - \frac{4}{3}\nu - \frac{17}{6}\Bigg\} \end{aligned} \tag{10}$$

3.2.2. *Bending energy of fully conformed graphene*

The bending energy of fully conformed graphene can be expressed as [43,44]

$$E_b = \int_{A'_g} \left[2B_M\left(C_M - \frac{C_0}{2}\right)^2 + B_G C_G\right] dA'_g \tag{11}$$

Here B_M and B_G are the bending rigidity and the Gaussian bending stiffness, respectively, and for single-layer graphene, they are obtained from the experimental [45] and first principle results [43,46–49] as $B_M = 1.45$ eV and $B_G = -1.1$ eV. $C_M = (k_1 + k_2)/2$ and $C_G = k_1 k_2$ are the average curvature and the Gaussian curvature, respectively, where k_1 and k_2 are the two principal curvatures of a 3-dimensional surface and are both equal to $R_g^{-1} \approx R_S^{-1}$ for spherical caps. C_0 is the spontaneous curvature and disappears for symmetrical surfaces.

Using Eqs. (3) and (11), the bending energy can be rewritten as

$$E_b = \pi\left(\frac{r_g}{R_S}\right)^2 (2B_M + B_G) \tag{12}$$

3.2.3. *Graphene-substrate adhesion energy*

The graphene-substrate interaction energy can be given via summing up all the interaction energies due to the van der Waals (VDW) force between the carbon atoms and the substrate atoms. Furthermore, since the interaction between the graphene and substrate atoms is weak and of short range, the main contribution to the interaction between the graphene and substrate comes from the upper layers of the substrate [36,50]. Our studies show that the total energy of system with only one layer substrate atoms is about 98% of the system consisting of four-layers substrate atoms (see Appendix B for details). Therefore, only the top layer substrate atoms are considered in the analysis, which can simplify the theoretical model and increase the computational efficiency greatly.

The adhesion energy E_{ad} between a graphene of area A'_g and a substrate of area A_S is

$$E_{ad} = \int_{A'_g} \int_{A_S} V(d)\rho_S dA_S \rho'_g dA'_g \tag{13}$$

where ρ'_g is the homogenized carbon atom area density of the conformed graphene. Based on the assumption of unchanged area, it can be obtained that $A'_g = A_g$ and $\rho'_g = \rho_g = 4/(3\sqrt{3}l_{C\text{-}C}^2)$, in which $l_{C\text{-}C}$ is the equilibrium carbon–carbon bond length. ρ_S is the density of substrate atoms and can be indicated by $\rho_S = N/(4\pi R_S^2)$, in which N is the number of spherical substrate atoms. $V(d)$ describes the VDW interactions between a carbon atom and a substrate atom with distance d, and can be characterized by the Lennard-Jones 6–12 potential as

$$V(d) = 4\varepsilon\left[\left(\frac{\sigma}{d}\right)^{12} - \left(\frac{\sigma}{d}\right)^{6}\right] \tag{14}$$

Here σ is the energy parameter and ε is the length parameter. For the SiO_2 substrate, they are 0.2935 nm and 0.00513 eV respectively [50].

In the graphene-substrate system, supposing the graphene conforms fully to the substrate with a uniform equilibrium distance h between the graphene and substrate, the distance between a carbon atom and a substrate atom is

$$d = \sqrt{R_S^2 + (R_S + h)^2 - 2R_S(R_S + h)\cos\theta} \tag{15}$$

The adhesion energy E_{ad} then yields as (see Appendix C for details)

$$E_{ad} = \frac{4\varepsilon\rho_S\pi R_S^2}{R_S(R_S+h)}\left[\frac{\sigma^6}{2(2R_S+h)^4} - \frac{\sigma^{12}}{5(2R_S+h)^{10}} + \frac{\sigma^{12}}{5h^{10}} - \frac{\sigma^6}{2h^4}\right]\rho'_g A'_g \tag{16}$$

Eq. (16) describes the adhesion energy between two fully conformed dome-shaped surfaces. It can easily degenerates into the adhesion energy between two flat surfaces by making $R_S \to +\infty$, which is exactly same as the result deduced by Zhu and Li [36] for a flat graphene on a flat substrate.

The equilibrium distance h in Eq. (16) can be obtained by minimizing the adhesion energy by $\partial E_{ad}/\partial h = 0$. For the spherical SiO_2 substrate with $R_S \gg h$, h is about 0.29 nm.

3.3. *Critical condition for full/partial conformation of graphene*

The total energy E_T of graphene-substrate system depends on the graphene radius r_g and substrate radius R_S, expressed as

$$\begin{aligned} E_T = E_m + E_b + E_{ad} = & \frac{2\pi R_S^2 t_g E}{(1-\nu^2)}\Bigg\{4(1+\nu)\left[\sqrt{1-\left(\frac{r_g}{2R_S}\right)^2} + \frac{1}{3}\left(\sqrt{1-\left(\frac{r_g}{2R_S}\right)^2}\right)^3\right] - \ln\left[1-\left(\frac{r_g}{2R_S}\right)^2\right] - \frac{1}{2}\left[1-\left(\frac{r_g}{2R_S}\right)^2\right]^2 \\ & - 2(1+2\nu)\left[1-\left(\frac{r_g}{2R_S}\right)^2\right] - \frac{4}{3}\nu - \frac{17}{6}\Bigg\} + \pi\left(\frac{r_g}{R_S}\right)^2(2B_M + B_G) \\ & + \frac{16\varepsilon\rho_S\pi^2 r_g^2 R_S}{3\sqrt{3}l_{C\text{-}C}^2(R_S+h)}\left[\frac{\sigma^6}{2(2R_S+h)^4} - \frac{\sigma^{12}}{5(2R_S+h)^{10}} + \frac{\sigma^{12}}{5h^{10}} - \frac{\sigma^6}{2h^4}\right] \end{aligned} \tag{17}$$

The real equilibrium state of the graphene sheet is determined by the competition between the strain energy of graphene ($E_m + E_b$) and the adhesion energy E_{ad}. The strain energy ($E_m + E_b$) results from the deformation of graphene and tries to keep the graphene sheet flat. On the other hand, the adhesion energy E_{ad} is the interaction between the graphene and the substrate, and it forces the graphene to conform to the substrate surface.

For a system with a very tiny graphene sheet, i.e. $r_g \ll R_S$, the substrate can be considered as flat, and the graphene sheet can easily conform fully to the substrate [35]. If the graphene radius increases to $r_g + dr_g$, the system total energy changes to $E_T(r_g + dr_g) = E_T(r_g) + \Delta E_T$, in which ΔE_T is the change in total energy due to the increased annulus area $2\pi r_g \cdot dr_g$. $\Delta E_T < 0$ indicates that the adhesion energy dominates the energy of the annulus and the graphene of $r_g + dr_g$ can conform to the substrate fully. And $\Delta E_T > 0$ means that the strain energy dominates the annulus and the annulus tends to leave away from the substrate. Therefore, conforming the graphene sheet with the radius of $r_g + dr_g$ fully to the substrate requires $E_T(r_g + dr_g) < E_T(r_g)$. Based on this analysis, the critical condition on full/partial conformation of graphene to the substrate can be established by

$$\frac{\partial E_T}{\partial r_g} = \frac{2\pi r_g E t_g}{(1-\nu^2)}\left\{-4(1+\nu)\left[\frac{1}{2\sqrt{4-\left(\frac{r_g}{R_S}\right)^2}} + \frac{\sqrt{4-\left(\frac{r_g}{R_S}\right)^2}}{8}\right] + \frac{1}{2\left[1-\left(\frac{r_g}{2R_S}\right)^2\right]} - \frac{1}{8}\left(\frac{r_g}{R_S}\right)^2 + \frac{3}{2} + 2\nu\right\} + \frac{2\pi r_g(2B_M + B_G)}{R_S^2} + \frac{32\varepsilon\rho_S\pi^2 r_g R_S}{3\sqrt{3}l_{C\text{-}C}^2(R_S+h)}\left[\frac{\sigma^6}{2(2R_S+h)^4} - \frac{\sigma^{12}}{5(2R_S+h)^{10}} + \frac{\sigma^{12}}{5h^{10}} - \frac{\sigma^6}{2h^4}\right] = 0 \quad (18)$$

Eq. (18) indicates that the graphene sheet conforms to the substrate fully when $\partial E_T/\partial r_g < 0$ and wrinkles if $\partial E_T/\partial r_g > 0$.

Taking $Et_g = 357$ N/m and $\nu = 0.186$ from the references [43,51], and $h = 0.29$ nm and $\rho_S = 0.181$/Å as discussed above for SiO_2 substrate, the critical radius of graphene sheet for an arbitrary specified substrate radius can be solved numerically from Eq. (18), as shown in Fig. 3 by the red curve.

In Fig. 3, the curve divides the R_S–r_g space into two regions: (1) in the region below the curve, $\partial E_T/\partial r_g < 0$, and thus the graphene can conform fully to the dome-shaped substrate; (2) in the region above the curve, $\partial E_T/\partial r_g > 0$, and thus the graphene cannot conform stably to the dome-shaped substrate and winkles appear in the graphene.

It is interesting to notice that the curve of this critical condition is almost linear, with a slope of

$$\left.\frac{r_g}{R_S}\right|_{\text{critical}} \approx 0.43 \quad (19)$$

So the critical value of the cone angle of the absorbed graphene ω can be obtained as

$$\omega_C = 2\arccos\left[1 - \frac{1}{2}\left(\left.\frac{r_g}{R_S}\right|_{\text{critical}}\right)^2\right] = 57.68^\circ \quad (20)$$

Eq. (20) implies that the critical value of the cone angle is a constant. For all the dome-shaped SiO_2 surfaces with cone angle $\omega < 57.68^\circ$, the graphene can conform fully to the surface. Conversely, wrinkles appear in the graphene if $\omega > 57.68^\circ$.

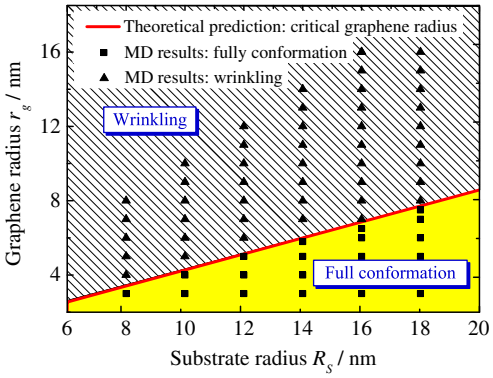

Fig. 3 – Phase diagram of the morphologies of a monolayer graphene sheet attached to the substrate. (A color version of this figure can be viewed online.)

4. Verification by molecular dynamics (MD) simulation

4.1. MD model

Molecular dynamics (MD) simulation is adopted to verify the theoretical result. In the atomistic model, all the substrate atoms are distributed evenly on the surface of the sphere with using the method proposed by Hardin et al.[a], and a round graphene sheet is placed on the top of the sphere substrate and parallel to the X–Y plane. SiO_2 is one of the most popular substrates in nano devices, and thus chosen as the substrate material. The substrate is considered as a rigid body.

All the MD simulations in this paper are performed with using the large-scale atomic molecular massively parallel simulator (LAMMPS) [52]. The adaptive intermolecular reactive empirical bond order (AIREBO) [53] is taken to describe interactions between carbon atoms, which has been verified to give a precise description of the properties of graphene, such as bond breaking and bond reforming of carbon atoms [54]. The cutoff parameter is taken as 0.192 nm for REBO potential [55]. In order to simulate the interactions between the graphene and the substrate, the Lennard-Jones potential with parameters $\sigma = 0.2935$ nm and $\varepsilon = 0.00513$ eV [50] is employed, which has been proved to be able to depict the two-type-atom system well. Constant temperature MD simulations are carried out at 5 K with NVT ensemble. The equations of motion are integrated using the Verlet leapfrog method with a time step of 2 fs. All the cases in this paper are run for 2 ns, which is a long enough time for the convergence of this problem. In the simulations, the energy of the systems remains unchanged after running about 300 ps. The morphology of the graphene sheet with unchanged total energy is regarded as the final stable morphology of the graphene sheet.

[a] Hardin RH, Sloane NJA, Smith WD. Tables of spherical codes with icosahedral symmetry. published electronically at http://NeilSloane.com/icosahedral.codes/.

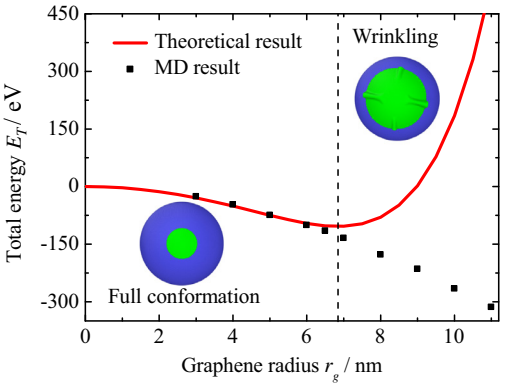

Fig. 4 – Comparison between theoretical and MD results on the total energy of the graphene-substrate system with the substrate radius R_S = 16 nm. (A color version of this figure can be viewed online.)

4.2. *Results and discussions*

First, the graphene-SiO_2 systems with a fixed substrate radius of $R_S = 16$ nm is studied. It can be easily estimated from the theoretical result in Eq. (18) that the critical radius of the graphene from full conformation to the wrinkling morphology is $r_g^C \approx 6.9$ nm. So MD simulations on the conformation behaviors of graphene sheets with radius ranging from 3 nm to 16 nm are carried out, and the total energy E_T of these systems calculated by Eq. (17) is plotted and compared with the MD result in Fig. 4. The simulated systems are relaxed for a sufficient time until a stable and minimum potential energy of the systems is achieved.

Defining the energy of the initial state of separate equilibrium is zero, the total energy E_T obtained from MD simulations agree well with the theoretical predictions when the graphene radius smaller than the critical radius r_g^C. While for the cases with the graphene radius larger than the critical radius r_g^C, the theoretical result is very different from the simulation results. This is because only full conformation morphology is taken into consideration in the theoretical model, and this theoretical model is not suitable for the systems with $r_g > r_g^C$. However, Fig. 4 presents clearly that the critical radius can be predicted accurately by the theoretical model.

Fig. 5 shows the final morphologies of the graphene sheets with different radius conforming to the substrate. Two different morphologies are presented clearly: (1) full conformation and (2) partial conformation with wrinkling. The wrinkles are generated in the process of absorbing energy of graphene through mechanical deformations [10]. It is obviously observed that the critical radius of the graphene from the full conformation state to the wrinkling state is between 6.5 and 7 nm, which is consistent well with the theoretical model, in which $r_g^C \approx 6.9$ nm (Figs. 3 and 4). Furthermore, it can be clearly observed from Fig. 5 that the amplitude and number of the wrinkles increase with the graphene radius. For the case shown in Fig. 5, when the graphene radius increases beyond the critical value, three small wrinkles appear, as presented in Fig. 5(d) and (e). Then, with increasing graphene radius, the amplitude of the wrinkles increases while the number of wrinkles remains. If the graphene radius keeps increasing, more new wrinkles with small amplitude are generated, as presented in Fig. 5(f), (g) and (h). Previous studies on the wrinkles of graphene have shown that the strain of graphene is the main reason for wrinkling [56]. In our study, according to the theoretical result in Eq. (8), the magnitude of the hoop compressive strain at the edge of graphene increases with the graphene radius, and becomes the main reason for the increasing in amplitude and number of the wrinkles. However, the mechanisms and rules of this increasing are still unrevealed and further investigation needs to be carried out, which is beyond the scope of this paper.

Similarly, for the spherical substrates with different radius R_S, the MD simulations can be conducted and the final morphologies can be observed. Thus, the morphology of each pair

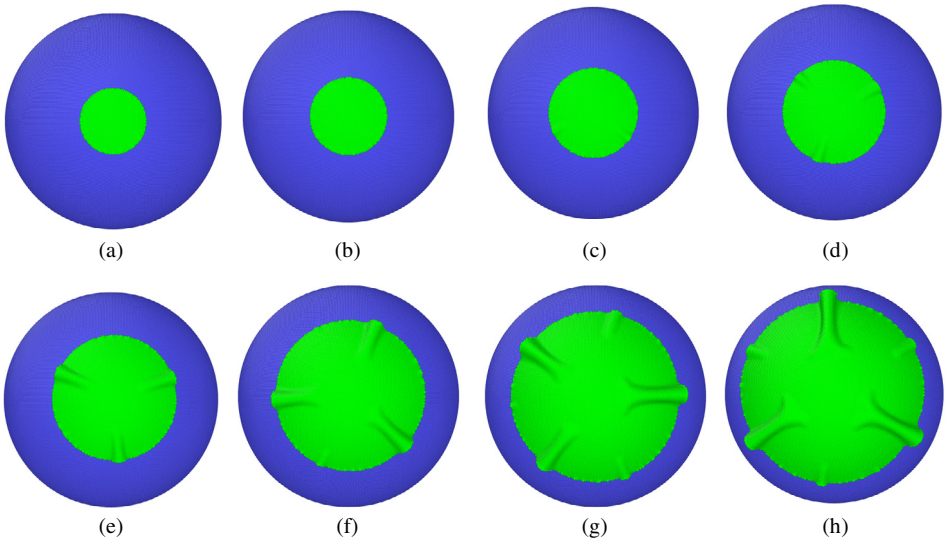

Fig. 5 – The equilibrium morphologies of graphene sheets with different radii on the substrate with radius of 16 nm: (a) r_g = 5 nm, (b) r_g = 6.5 nm, (c) r_g = 7 nm, (d) r_g = 8 nm, (e) r_g = 10 nm, (f) r_g = 12 nm, (g) r_g = 14 nm, (h) r_g = 16 nm. (A color version of this figure can be viewed online.)

of (R_S, r_g) is obtained and presented in Fig. 3. It can be found from Fig. 3 that all the full conformation cases are located in the region below the dividing curve obtained from theoretical analysis, and all the wrinkling cases are above the curve. This good agreement between MD and theoretical results illustrates the validity of the theoretical model. Accordingly, the criterion curve in Fig. 3, as well as the criterion of cone angle in Eq. (20), which is obtained from linearization of the criterion curve in Fig. 3, can both be used to decide the final morphology of a monolayer graphene sheet on the substrate with dome-shaped bumps.

Using the full/partial conformation criterion established in Eq. (20) or Fig. 3, the phenomenon in Fig. 1 can be easily explained. Although the heights and distances of the bumps on the two surfaces are same, the cone angles are different. The cone angle in Fig. 1(a) is 54°, a little smaller than the critical cone angle ω_C (57.68°), while that in Fig. 1(b) is 61°, a little larger than ω_C. So the former can conform fully to the graphene sheet and the latter cannot.

It should be pointed out that the theoretical prediction on the independence of the critical absorbed cone angle and linear relation between the critical graphene radius and the substrate radius are still hold for substrates with different parameters of the Lennard-Jones potentials for van der Waals interactions. The SiO_2 substrate is just an example to show the full-conformation/wrinkling criterion because it is commonly-used in the coating materials. Furthermore, the criterion established in Eq. (20) is independent of size, which means it is applicable for not only nano-scale but also micro-scale roughness.

5. Conclusions and discussions

To establish a criterion deciding the configurations of a monolayer graphene sheet adsorbed by substrates with nano and micro-roughness, an energy-based theoretical model is developed, in which the adhesion energy and the strain energy are taken into account to describe the competing mechanism between full conformation and wrinkling. The theoretical solution is verified perfectly by MD simulations, achieving the following outcomes.

The full-conformation/wrinkling criterion can be expressed as a function of the graphene size and radius of substrate curvature (Eq. (18)), which are thus the two dominating parameters on the morphology of graphene. Accordingly the criterion can be presented in the two dimensional space of the two dominating parameters (Fig. 3). Using this criterion, for a spherical substrate with a given curvature, the maximum radius of fully conformed graphene sheet can be easily attained, and the graphene sheet wrinkles if it larger than the maximum size. This is very helpful for the decision on the sheet size in electronic eye cameras, as well as the size of coating graphenes on the AFM tip. One the other hand, for a graphene sheet with a given radius, the minimum radius of substrate curvature can also be easily obtained by the full-conformation/wrinkling criterion.

Furthermore, it is amazing to find that the two dominate parameters can be reduced into one, the cone angle of the dome-shaped substrate. A critical cone angle of $\omega_C = 57.68°$ is obtained for SiO_2 substrate based on our theoretical analysis. Graphene sheet conforms to the substrate fully and smoothly when $\omega < 57.68°$, while wrinkles appear in the graphene when $\omega > 57.68°$. Therefore, the final morphology of the adsorbed graphene sheets is dominated by the cone angle only, which means whether the graphene sheet can fully conform to a substrate with roughness depends only on the cone angle of the bumps.

This work can be used to make active and precise prediction and control on the graphene conformation to substrates with asperities and substrates with spherical surfaces, which could provide guidance to fabricate high quality nanostructured coatings. Besides, the critical state between wrinkling and full conformation can be utilized to design new nanoelectronic devices, such as nano-sensors and nano-switches.

Acknowledgments

The authors thank the support from the National Natural Science Foundation of China (Nos. 11202012, 11472027 and 11372158), the Program for New Century Excellent Talents in University (No. NCET-13-0021), the Fundamental Research Funds for the Central Universities, and the Beijing Higher Education Young Elite Teacher Project. We also thank Dr. Ran Xu, Mr. Tao Wang, Mr. Zeshuai Yuan and Mr. Yong Ma for discussions.

Appendix A

The areas of the graphene sheet in both the initial flat state and the final conformed state are plotted in Fig. A. It can be found that the areas of graphene are almost constant when the graphene conforms to the substrate fully. The maximum variation between the initial and conformed states is about 0.64% for the full conformation cases (green scatters). So it is appropriate to assume that the area of graphene sheet keeps constant when it conforms fully to a substrate.

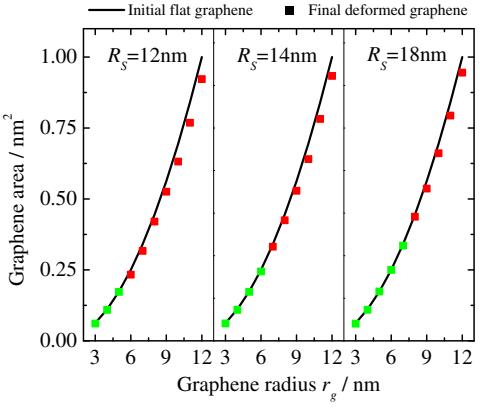

Fig. A – The area of graphene sheets at the initial (the solid line) and equilibrium (the scatters) states. The green scatters denote the full conformation cases, and the red ones represent the wrinkling cases. (A color version of this figure can be viewed online.)

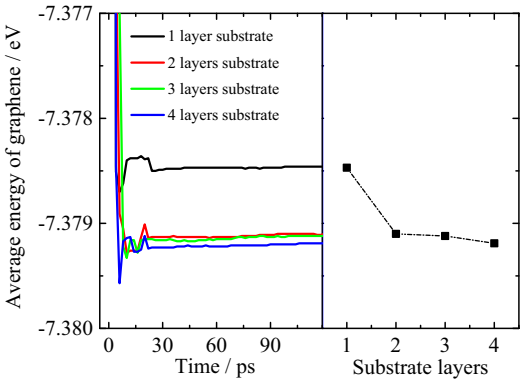

Fig. B – The energy of the graphene-substrate system with various substrate layers. (A color version of this figure can be viewed online.)

Appendix B

The systems including a monolayer graphene sheet and complanate substrates with 1–4 atomic layers and the same atomic density as the spherical substrate are set up. The total energy of the systems in their equilibrium states is obtained by using molecular dynamics, and presented in Fig. B. It is found that the total energy of system with only one layer substrate atoms is about 98% of the system consisting of four layers substrate atoms, and the latter system has the thickness larger than the cut-off radius of the simulations. This motivates us to restrict our investigations to the top layer substrate atoms, which can help us increase the computational efficiency greatly.

Appendix C

The monographene sheet is assumed to be absorbed on the substrate with a distance of h between the graphene sheet and the substrate. Accordingly, every atom of the graphene is over the substrate with the distance h. Thus, for an infinitesimal graphene area dA'_g, the corresponding adhesion energy dE_{ad} can be obtained from Eqs. (13)–(15) as

$$\begin{aligned} dE_{ad} &= 4\varepsilon\rho'_g dA'_g \int \left(\frac{\sigma^{12}}{\left(R_S^2+(R_S+h)^2-2R_S(R_S+h)\cos\theta\right)^6} \right. \\ &\quad \left. - \frac{\sigma^6}{\left(R_S^2+(R_S+h)^2-2R_S(R_S+h)\cos\theta\right)^3} \right) \rho_S dA_S \\ &= 4\varepsilon\rho'_g dA'_g \int \left(\frac{\sigma^{12}}{\left(R_S^2+(R_S+h)^2-2R_S(R_S+h)\cos\theta\right)^6} \right. \\ &\quad \left. - \frac{\sigma^6}{\left(R_S^2+(R_S+h)^2-2R_S(R_S+h)\cos\theta\right)^3} \right) \rho_S 2\pi R_S^2 \sin\theta d\theta \\ &= \frac{4\varepsilon\rho_S\pi R_S^2}{R_S(R_S+h)} \left[\frac{\sigma^6}{2(2R_S+h)^4} - \frac{\sigma^{12}}{5(2R_S+h)^{10}} + \frac{\sigma^{12}}{5h^{10}} - \frac{\sigma^6}{2h^4} \right] \rho'_g dA'_g \end{aligned} \quad \text{(C1)}$$

Then, the adhesion energy between the whole graphene and substrate can be given as

$$\begin{aligned} E_{ad} &= \int_{A'_g} \frac{4\varepsilon\rho_S\pi R_S^2}{R_S(R_S+h)} \left[\frac{\sigma^6}{2(2R_S+h)^4} - \frac{\sigma^{12}}{5(2R_S+h)^{10}} + \frac{\sigma^{12}}{5h^{10}} - \frac{\sigma^6}{2h^4} \right] \rho'_g dA'_g \\ &= \frac{4\varepsilon\rho_S\pi R_S^2}{R_S(R_S+h)} \left[\frac{\sigma^6}{2(2R_S+h)^4} - \frac{\sigma^{12}}{5(2R_S+h)^{10}} + \frac{\sigma^{12}}{5h^{10}} - \frac{\sigma^6}{2h^4} \right] \rho'_g A'_g \end{aligned} \quad \text{(C2)}$$

REFERENCES

[1] Novoselov K, Geim AK, Morozov S, Jiang D, Katsnelson M, Grigorieva I, et al. Two-dimensional gas of massless Dirac fermions in graphene. Nature 2005;438(7065):197–200.

[2] Bunch JS, Van Der Zande AM, Verbridge SS, Frank IW, Tanenbaum DM, Parpia JM, et al. Electromechanical resonators from graphene sheets. Science 2007;315(5811):490–3.

[3] Lee C, Wei X, Kysar JW, Hone J. Measurement of the elastic properties and intrinsic strength of monolayer graphene. Science 2008;321(5887):385–8.

[4] Chou S, Wang J, Choucair M, Liu H, Stride JA, Dou S. Enhanced reversible lithium storage in a nanosize silicon/graphene composite. Electrochem Commun 2010;12(2):303–6.

[5] Zhang H, Lv X, Li Y, Wang Y, Li J. P25-graphene composite as a high performance photocatalyst. ACS Nano 2009;4(1):380–6.

[6] Meyer JC, Geim AK, Katsnelson MI, Novoselov KS, Booth TJ, Roth S. The structure of suspended graphene sheets. Nature 2007;446(7131):60–3.

[7] Merino P, Svec M, Pinardi AL, Otero G, Martín-Gago JA. Strain-driven moiré superstructures of epitaxial graphene on transition metal surfaces. ACS Nano 2011;5(7):5627–34.

[8] Van Gastel R, Martínez-Galera AJ, Coraux J, Hattab H, Wall D, Zu Heringdorf FM, et al. In situ observation of stress relaxation in epitaxial graphene. New J Phys 2009;11(11):113056.

[9] Hattab H, Diaye ATN, Wall D, Klein C, Jnawali G, Coraux J, et al. Interplay of wrinkles, strain, and lattice parameter in graphene on iridium. Nano Lett 2012;12(2):678–82.

[10] Chae SJ, Güneş F, Kim KK, Kim ES, Han GH, Kim SM, et al. Synthesis of large-area graphene layers on poly-nickel substrate by chemical vapor deposition: wrinkle formation. Adv Mater 2009;21(22):2328–33.

[11] Ishigami M, Chen JH, Cullen WG, Fuhrer MS, Williams ED. Atomic structure of graphene on SiO_2. Nano Lett 2007;7(6):1643–8.

[12] Geringer V, Liebmann M, Echtermeyer T, Runte S, Schmidt M, Rückamp R, et al. Intrinsic and extrinsic corrugation of monolayer graphene deposited on SiO_2. Phys Rev Lett 2009;102(7):76102.

[13] Li H, Zhao Q, Wang W, Dong H, Xu D, Zou G, et al. Novel planar-structure electrochemical devices for highly flexible semitransparent power generation/storage sources. Nano Lett 2013;13(3):1271–7.

[14] Lanza M, Gao T, Yin Z, Zhang Y, Liu Z, Tong Y, et al. Nanogap based graphene coated AFM tips with high spatial resolution, conductivity and durability. Nanoscale 2013;5(22):10816–23.

[15] Neto AC, Guinea F, Peres N, Novoselov KS, Geim AK. The electronic properties of graphene. Rev Mod Phys 2009;81(1):109.

[16] Morozov SV, Novoselov KS, Katsnelson MI, Schedin F, Ponomarenko LA, Jiang D, et al. Strong suppression of weak localization in graphene. Phys Rev Lett 2006;97(1):16801.

[17] Ferrari AC, Meyer JC, Scardaci V, Casiraghi C, Lazzeri M, Mauri F, et al. Raman spectrum of graphene and graphene layers. Phys Rev Lett 2006;97(18):187401.

[18] Stolyarova E, Rim KT, Ryu S, Maultzsch J, Kim P, Brus LE, et al. High-resolution scanning tunneling microscopy imaging of

mesoscopic graphene sheets on an insulating surface. Proc Natl Acad Sci 2007;104(22):9209–12.
[19] Wei Y, Wu J, Yin H, Shi X, Yang R, Dresselhaus M. The nature of strength enhancement and weakening by pentagon–heptagon defects in graphene. Nat Mater 2012;11(9):759–63.
[20] Katsnelson MI, Geim AK. Electron scattering on microscopic corrugations in graphene. Philos T R Soc A 1863;2008(366):195–204.
[21] Zhu W, Low T, Perebeinos V, Bol AA, Zhu Y, Yan H, et al. Structure and electronic transport in graphene wrinkles. Nano Lett 2012;12(7):3431–6.
[22] Lui CH, Liu L, Mak KF, Flynn GW, Heinz TF. Ultraflat graphene. Nature 2009;462(7271):339–41.
[23] Dean CR, Young AF, Meric I, Lee C, Wang L, Sorgenfrei S, et al. Boron nitride substrates for high-quality graphene electronics. Nat Nanotech 2010;5(10):722–6.
[24] Ko HC, Stoykovich MP, Song J, Malyarchuk V, Choi WM, Yu C, et al. A hemispherical electronic eye camera based on compressible silicon optoelectronics. Nature 2008;454(7205):748–53.
[25] Decker R, Wang Y, Brar VW, Regan W, Tsai H, Wu Q, et al. Local electronic properties of graphene on a BN substrate via scanning tunneling microscopy. Nano Lett 2011;11(6):2291–5.
[26] Boukhvalov DW, Katsnelson MI. Enhancement of chemical activity in corrugated graphene. J Phys Chem C 2009;113(32):14176–8.
[27] Boukhvalov DW. Tuneable molecular doping of corrugated graphene. Surf Sci 2010;604(23):2190–3.
[28] Zhang Y, Fu Q, Cui Y, Mu R, Jin L, Bao X. Enhanced reactivity of graphene wrinkles and their function as nanosized gas inlets for reactions under graphene. Phys Chem Chem Phys 2013;15(43):19042–8.
[29] Kimouche A, Renault O, Samaddar S, Winkelmann C, Courtois H, Fruchart O, et al. Modulating charge density and inelastic optical response in graphene by atmospheric pressure localized intercalation through wrinkles. Carbon 2014;68:73–9.
[30] Politano A, Chiarello G. Periodically rippled graphene on Ru (0001): a template for site-selective adsorption of hydrogen dimers via water splitting and hydrogen-spillover at room temperature. Carbon 2013;61:412–7.
[31] Wang B, Günther S, Wintterlin J, Bocquet ML. Periodicity, work function and reactivity of graphene on Ru (0001) from first principles. New J Phys 2010;12(4):43041.
[32] Li T, Zhang Z. Substrate-regulated morphology of graphene. J Phys D Appl Phys 2010;43(7):75303.
[33] Li T. Extrinsic morphology of graphene. Model Simul Mater Sci 2011;19(5):54005.
[34] Gao W, Huang R. Effect of surface roughness on adhesion of graphene membranes. J Phys D Appl Phys 2011;44(45):452001.
[35] Chen H, Yao Y, Chen S. Adhesive contact between a graphene sheet and a nano-scale corrugated surface. J Phys D Appl Phys 2013;46(20):205303.
[36] Zhu S, Li T. Wrinkling instability of graphene on substrate-supported nanoparticles. J Appl Mech 2014;81(6):61008.
[37] Yamamoto M, Pierre-Louis O, Huang J, Fuhrer MS, Einstein TL, Cullen WG. "The Princess and the Pea" at the nanoscale: wrinkling and delamination of graphene on nanoparticles. Phys Rev X 2012;2(4):41018.
[38] Yin Q, Shi X. Mechanics of rolling of nanoribbon on tube and sphere. Nanoscale 2013;5(12):5450–5.
[39] Osváth Z, Gergely-Fülöp E, Nagy N, Deák A, Nemes-Incze P, Jin X, et al. Controlling the nanoscale rippling of graphene with SiO_2 nanoparticles. Nanoscale 2014;2(6):6030–6.
[40] Liu N, Pan Z, Fu L, Zhang C, Dai B, Liu Z. The origin of wrinkles on transferred graphene. Nano Res 2011;4(10):996–1004.
[41] Majidi C, Fearing RS. Adhesion of an elastic plate to a sphere. Proc R Soc A 2008;464(2093):1309–17.
[42] Hure J, Roman B, Bico J. Wrapping an adhesive sphere with an elastic sheet. Phys Rev Lett 2011;106(17):174301.
[43] Wei Y, Wang B, Wu J, Yang R, Dunn ML. Bending rigidity and Gaussian bending stiffness of single-layered graphene. Nano Lett 2012;13(1):26–30.
[44] Lipowsky R. The conformation of membranes. Nature 1991;349(6309):475–81.
[45] Nicklow R, Wakabayashi N, Smith HG. Lattice dynamics of pyrolytic graphite. Phys Rev B 1972;5(12):4951.
[46] Sánchez-Portal D, Artacho E, Soler JM, Rubio A, Ordejón P. Ab initio structural, elastic, and vibrational properties of carbon nanotubes. Phys Rev B 1999;59(19):12678.
[47] Kudin KN, Scuseria GE, Yakobson BI. C 2 F, BN, and C nanoshell elasticity from ab initio computations. Phys Rev B 2001;64(23):235406.
[48] Muñoz E, Singh AK, Ribas MA, Penev ES, Yakobson BI. The ultimate diamond slab: GraphAne versus graphene. Diam Relat Mater 2010;19(5):368–73.
[49] Koskinen P, Kit OO. Approximate modeling of spherical membranes. Phys Rev B 2010;82(23):235420.
[50] Neek-Amal M, Peeters FM. Strain-engineered graphene through a nanostructured substrate. I. Deformations. Phys Rev B 2012;85(19):195445.
[51] Politano A, Marino AR, Campi D, Farías D, Miranda R, Chiarello G. Elastic properties of a macroscopic graphene sample from phonon dispersion measurements. Carbon 2012;50(13):4903–10.
[52] Plimpton S. Fast parallel algorithms for short-range molecular dynamics. J Comput Phys 1995;117(1):1–19.
[53] Stuart SJ, Tutein AB, Harrison JA. A reactive potential for hydrocarbons with intermolecular interactions. J Chem Phys 2000;112(14):6472–86.
[54] Zhao H, Aluru NR. Temperature and strain-rate dependent fracture strength of graphene. J Appl Phys 2010;108(6):64321.
[55] Belytschko T, Xiao SP, Schatz GC, Ruoff RS. Atomistic simulations of nanotube fracture. Phys Rev B 2002;65(23):235430.
[56] Duan WH, Gong K, Wang Q. Controlling the formation of wrinkles in a single layer graphene sheet subjected to in-plane shear. Carbon 2011;49(9):3107–12.